Water Science & Technology

IWA PUBLISHING

Water Science & Technology Vol 88 No 6, 1547 doi: 10.2166/wst.2023.285

Nanocomposites from spent coffee grounds and iron/zinc oxide: green synthesis, characterization, and application in textile wastewater treatment

J. A. Reyes-Pérez[a], G. Roa-Morales[b], C. A. De León-Condes [a,*] and P. Balderas-Hernández[b]

[a] Tecnológico Nacional de México/ TES de Tianguistenco, Km. 22, Carretera Tenango – La Marquesa Santiago Tilapa, Santiago Tianguistenco 52650, México
[b] Universidad Autónoma del Estado de México, (UAEMex), Centro Conjunto de Investigación en Química Sustentable (CCIQS) UAEM-UNAM, Carretera Toluca-Atlacomulco, Km 14.5, Toluca, MEX 50200, México
*Corresponding author. E-mail: deleoncondes@yahoo.com

CAD, 0000-0002-7719-4048

ABSTRACT

This study reports on a novel composite of bimetallic FeO/ZnO nanoparticles supported by spent coffee grounds (SCGs). The leaves of eucalyptus (*Eucalyptus globulus* Labill) and trumpet (*Cuphea aequipetala* Cav), with their high antioxidant content, serve as bio-reductant agents for the green synthesis of nanoparticles. It was characterized using Fourier transform infrared spectroscopy (FTIR), scanning electron microscopy (SEM), energy dispersive X-ray spectroscopy (EDS), X-ray diffraction (XRD), and transmission electron microscopy (TEM). Stable nanoparticles were produced with different diameters of 5–30 nm, and they were applied as catalysts in Fenton-like processes. Box–Behnken experimental design (BBD) was used to determine the optimal removal efficiency with three factors and was used in the degradation of textile dyes from wastewater. The nanocomposite displayed a high decolorization ratio (88%) of indigo carmine in the presence of H_2O_2 combined. This resulted in a reduction in chemical oxygen demand (COD) of 56% at 120 min of contact time at an initial pH of 3.0 and a 0.5 g/L of catalyst dose, a H_2O_2 concentration of 8.8 mM/L, an initial dye concentration of 100 mg/L, and a temperature of 25 °C.

Key words: composite, Fenton-like reaction, FeO/ZnO nanoparticles, green synthesis

HIGHLIGHTS

- Green synthesis of FeO/ZnO NPs using eucalyptus (*Eucalyptus globulus* Labill) and trumpet (*Cuphea aequipetala* Cav) extract was done.
- The process was optimized using a Box–Behnken design.
- UV–Visible spectroscopy, SEM, XRD, and TEM were done to analyze the structure morphology, size, and shape of nanoparticles.
- Nanocomposite of bimetallic FeO/ZnO was used for the removal of indigo carmine supported by spent coffee grounds (SCGs).

GRAPHICAL ABSTRACT

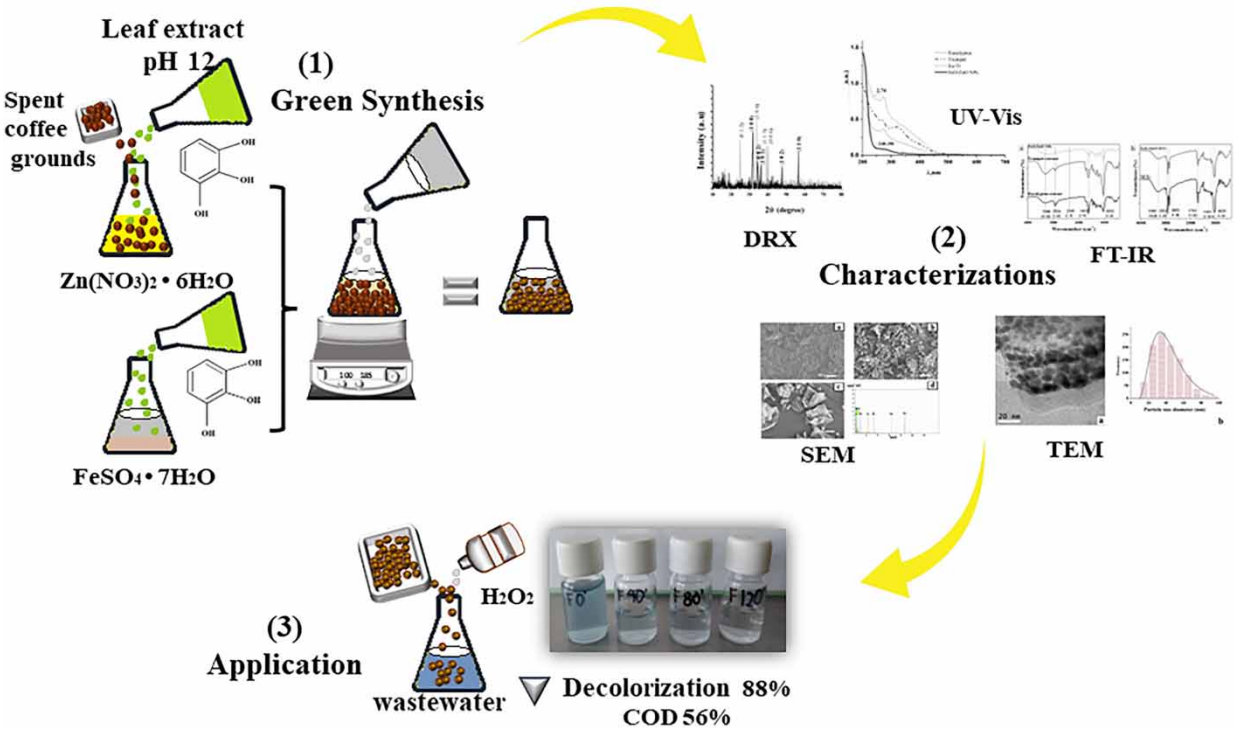

1. INTRODUCTION

The textile industry is one of the largest consumers of industrial water and producers of effluents in the world. The dye concentration of textile effluents varies widely (Azanaw *et al.* 2022). In addition, these industries have high concentrations of chemical oxygen demand (COD), biochemical oxygen demand (BOD), total suspended solids (TSS), temperature, and salts (Yaseen & Scholz 2019). The discharge of dyed effluents negatively affects ecosystems because they inhibit the penetration of sunlight, generating environmental problems (Ardila-leal *et al.* 2021). Indigo carmine dye, also known as 5,5′-indigodisulfonic acid disodium salt, is classified as a vat dye and is a basic organic blue dye that has been used in the textile industry (Benkhaya *et al.* 2020). It is a commercially available dye and is cheap and stable, but it is also hazardous to human health and highly soluble in aqueous solutions. Currently, its main consumption is in the blue jeans industry, with an annual production that exceeds 120,000 tons (Hevira *et al.* 2020; Cesur Özcan & Gürel 2023). Some treatment methods that have been used in the decolorization of indigo carmine such as ozonation (Peramune *et al.* 2022), electrocoagulation (Oliveira *et al.* 2020), and filtration, are efficient at removing dye, but present equipment problems and high energy consumption (Mousset *et al.* 2021).

The use of nanotechnology has gained prominence owing to technological advancements and the use of a variety of nanomaterials such as nanotubes, nanocomposites, nanofilters, and nanoparticles (NPs) to build systems and have significant applications in environmental issues. Some of these drawbacks, for example, carbon nanotubes are related to the difficulty of producing them without defects and their high cost of production (Aghababai Beni & Jabbari 2022; Elsehly *et al.* 2023).

Specifically, NPs are used due to their properties related to high surface area, which often makes them stand out from other bulk materials (Kumar *et al.* 2021). Furthermore, it is possible to overcome the limitations of conventional treatment technologies and employ safe, cheap, and non-toxic methods in their synthesis. Various physicochemical methods have been employed for the synthesis of metallic NPs, but the synthesis of these NPs through environmentally benign methods is more attractive and promising due to the production of non-toxic, cost-effective, and high-quality NPs (Nair *et al.* 2022). Plants have been considered the best choice to reduce metal ions and are ideal candidates for large-scale production; their phytochemicals like terpenes, flavones, ketones, aldehydes, amides, and carboxylic acids can be utilized as reducing and capping agents, minimizing the agglomeration and oxidation of NPs (Albeladi *et al.* 2020; Nasrollahzadeh *et al.* 2020). Leaf extracts from eucalyptus (*Eucalyptus globulus* Labill.) and trumpet (*Cuphea aequipetala* Cav.) contain phenolic compounds

such as syrupic acid, epicatechin, quercetin, gallic acid, robustaol B, and eucalyptin, among other polyphenols (Martınez-Bonfil *et al.* 2014; Vitta *et al.* 2020). Polyphenols are powerful antioxidants and free radical scavengers. Iron NPs can be prepared using plant extracts (polyphenols and caffeine) as intrinsic reductants and dispersants (Xiao *et al.* 2020). Many researchers have employed a green synthesis process for the preparation of metal/metal oxide NPs, such as iron and zinc, via plant leaf extracts (Katata-Seru *et al.* 2018; Jiménez-Rosado *et al.* 2022).

Zinc oxide (ZnO) NPs with iron oxide allow for obtain a material with improved photocatalytic properties, due to the addition of iron oxide, which reduces the width of the energy gap (Długosz *et al.* 2021; Elsehly *et al.* 2023; Sun *et al.* 2023). Zinc and iron oxide NPs have the ability to oxidize organic compounds, which makes them applicable for wastewater treatment (Aragaw *et al.* 2021). The application of supported NPs enables the reaction to be fast due to increased surface area and active sites. Therefore, NPs are able to work at low concentrations, reducing the amount of catalyst compared to that applied in conventional treatment. In the case of ZnO NPs, modifying them with other elements like iron increases their photocatalytic performance under visible light irradiation. The combination of two different metallic elements effectively improves the efficiency of nanomaterials through their individual metallic properties and the new properties that arise due to the synergistic effect (Scaria *et al.* 2020; Ferrier *et al.* 2022; Liang *et al.* 2022). Therefore, they may be useful for water and wastewater treatment, especially for recalcitrant contaminants, and thus could contribute to sustainable solutions to the water crisis (Scaria *et al.* 2020).

Coffee is a global consumer product; the annual global coffee consumption is about 8 million tons, and this consumption grows at an annual rate of 1.5% (Jin *et al.* 2018). Spent coffee grounds (SCGs), which are composed primarily of macromolecular cellulose and lignocellulose, can be used in sustainable processes and bioproducts due to their large amount of stock and renewability (Mangindaan *et al.* 2020). Six million tons of such residues are produced every year, according to the coffee trade record from the International Coffee Organization. The coffee extract could be used as a green reductant for synthesizing metallic NPs and function as a support material for heterogeneous reactions (Chien *et al.* 2019; Wu *et al.* 2019). In this paper, a novel composite was obtained with iron/zinc oxide nanoparticles (FeO/ZnO NPs) supported by SCGs. This nanomaterial was assayed for the degradation of indigo carmine in wastewater using a Fenton-like process.

2. MATERIALS AND METHODS

2.1. Materials

Zinc nitrate [$Zn(NO_3)_2 \cdot 6H_2O$] purity 99.1%, ferrous sulfate [$FeSO_4 \cdot 7H_2O$] purity 100%, and hydrogen peroxide 30% reagent grade were acquired from Fermont, indigo carmine dye from chemical reagents HYCEL, and for pH adjustment, a 4 M of sulfuric acid solution and a 2 M of NaOH solution were used. Eucalyptus (*E. globulus* Labill) and trumpet (*C. aequipetala* Cav) leaves were purchased at the local market from Metepec, State of Mexico. SCGs were donated by a local coffee shop. This is a residue with a fine particle size obtained during the treatment of raw coffee powder with hot water during the preparation of coffee. The coffee beans were of Mexican origin.

2.2. Green synthesis of FeO/ZnO + SCG composites

2.2.1. Preparation of *eucalyptus–trumpet* extract

Eucalyptus and trumpet leaves were washed several times with tap water to remove dust and any additional waste and were subsequently dried in the oven at 100 °C for 2 h, after which they were finely crushed and powdered with a mortar and pestle. The plants' extract was prepared following the method reported by Nagar & Devra (2018) and Siripireddy & Mandal (2017). 2.5 g of each plant were weighed and combined to obtain a total of 5 g, which was subsequently added to a beaker with 100 mL of distilled water. This mixture was then brought to a boil for 10 min and mixed using a magnetic stirrer before being filtered with standard filter paper to obtain the extract. The filtrate was used immediately for the biosynthesis of FeO/ZnO NPs.

2.2.2. Preparation of the FeO/ZnO + SCG composite

For the biosynthesis of Zn/Fe oxide, 20 mL of 0.05 M $Zn(NO_3)_2$ and 20 mL of 0.02 M $FeSO_4$ were prepared. The reduction reaction was carried out in two steps: first, 2 g of SCG were weighed, washed, and placed in a 50-mL beaker, to which 20 mL of the $Zn(NO_3)_2$ solution was added, before being constantly stirred for 2 h. Separately, 20 mL of infusion was separated, and its pH of 12 was adjusted. This infusion was added to the zinc solution with the SCG, and the temperature was raised to 100 °C for 1 h. Subsequently, another 20 mL of the eucalyptus–trumpet extract infusion were added without pH adjustment,

immediately followed by 20 mL of iron solution. The mixture was then constantly stirred for 1 h before being left undisturbed for 24 h, and then filtered through a standard filter paper, rinsed with distilled water, dried in the oven at 100 °C, placed in an airtight container, and reserved for later use.

2.2.3. Characterization FeO/ZnO + SCG composite

UV–vis spectral analysis was performed using the VELAB VE-5600UV PC UV–visible spectrophotometer, where the spectrum corresponding to the surface plasmon resonance (SPR) typical of FeO and ZnO NPs was identified. The absorption of the sample was recorded at wavelengths ranging from 200 to 900 nm, at a resolution of 1 nm, with 1 cm long quartz cuvettes.

The Fourier transform infrared (FTIR) analysis was performed using the Bruker Tensor 27 Fourier transform infrared spectrometer with an MIR source with the Bruker platinum ATR accessory with diamond glass to identify the functional groups present. The spectra were obtained in the infrared region between 4,000 and 400 cm^{-1}. The material surface analysis and morphology of the biosynthesized NPs were studied using the JEOL JSM-6510LV scanning electron microscope (SEM), which was coupled with an X-ray detector in order to perform chemical analysis by means of energy dispersion (EDS), Oxford, with a resolution of 137 eV. The NP sizes were determined using transmission electron microscopy (TEM) on evaporated drops from the reaction mixture placed over carbon-coated grids. TEM observations were performed on a JEOL 2100 TEM operated at a 200 kV accelerating voltage with a LaB6 source. X-ray powder diffraction (XRD) was performed using XRD Rigaku/Ultima-IV equipment with Cu-kα radiation (1.5406 Å) at 45 kV and a scanning speed of 2°/min. The pHpzc of the FeO/ZnO + SCG composite was determined using the procedure as follows: 50 mL of distilled water was taken in 100 mL of Erlenmeyer flasks, adjusting the pH of each solution between 2 and 8 units, adding the appropriate amounts of 0.1 M of HCl and 0.1 M NaOH, a fixed dose of 10 mg composite. The mixture was shaken at 170 rpm for 48 h. Then, the samples were centrifuged, and the pH of each solution was measured (Farrokhi *et al.* 2014).

2.3. Experimental design and optimization

Optimization is one of the essential steps in both the development of a synthesis protocol and the evaluation of the interaction of reaction parameters influencing the biosynthesis. An experimental response surface Box–Behnken design was realized using the Minitab Ver. 19.0 statistical package. In order to optimize the Fenton-like process with the FeO/ZnO + SCG catalyst, three factors were considered with two levels each and six central points in duplicate, obtaining a total of 30 runs; the dye concentration, amount of catalyst, and amount of hydrogen peroxide were considered independent variables, while the percentage of dye removal was considered a dependent or response variable. The values of the independent variables were selected based on the literature that was previously reviewed during research carried out for the removal of dyes through Fenton and Fenton-like processes (Hassani *et al.* 2018; Nadeem *et al.* 2020; Bel *et al.* 2021); the obtained matrix can be observed in Table 1. The initial conditions of the experiments were a volume of 10 mL and a pH of 3.0 adjusted with a 0.1 M sulfuric acid solution at a reaction time of 120 min.

The percentage of dye removal was monitored every 15 min throughout the reaction, taking as a sample a 100 µL aliquot that was diluted and read using UV–Vis spectrophotometry with the HACH DR 4000 U spectrophotometer, using Equation (1) at the characteristic maximum absorbance of indigo carmine (610 nm).

$$\text{Decolorization } (\%) = \frac{(A_0 - A_t)}{A_0} * 100 \quad (1)$$

2.4. Textile dyeing wastewater sample

The textile industry effluents used in the present study were collected from Mohammedia in Almoloya del Río, State of Mexico, and contain a mixture of compounds, with indigo carmine as the main dye.

Once the optimal conditions were obtained, they were tested with a sample of textile wastewater. The wastewater treatment was performed in a beaker with 0.5 g/L of FeO/ZnO + SWPS added to 100 mL of IC aqueous solution (pH = 3.1), H_2O_2 concentration 8.8 mM/L, under constant stirring for 60 min to achieve equilibrium. Subsequently, it was placed under direct sunlight (651–787 W/m^2 in Toluca, México) for 60 min of contact time.

Table 1 | Experimental design using the Box–Behnken design

	Variables		
Run number	Dye concentration (mg/L)	Catalyst (mg)	H_2O_2 (μL)
1	50	5	4
2	100	5	4
3	50	10	4
4	100	10	4
5	50	7.5	3
6	100	7.5	3
7	50	7.5	5
8	100	7.5	5
9	75	5	3
10	75	10	3
11	75	5	5
12	75	10	5
13	75	7.5	4
14	75	7.5	4
15	75	7.5	4

2.5. Analytical methods

The sample was characterized by determined parameters such as pH, conductivity, turbidity, and COD in accordance with the procedures established in the Standard Methods for the Examination of Water and Wastewater, 2012 edition. The dye removal was measured through UV–visible spectrophotometry with the VE-5600UV PC spectrophotometer, using Equation (1) at the maximum absorbance of the sample.

3. RESULTS AND DISCUSSION

3.1. Analysis of the biosynthesized FeO/ZnO + SCG composite

3.1.1. UV–visible study

In the case of the reaction of zinc with the bioreducing components of the infusion of eucalyptus and trumpet (Eu-Tr), the formation of a precipitate is observed, while adding the iron changes the whole solution's dye to black, corroborating the formation of the NPs. UV–visible spectrophotometry was achieved, where the absorption bands of the surface plasmon resonance (SPR), which are characteristic of the NPs, were observed. In Figure 1, the gray solid line shows the spectrum of the mixed infusions of eucalyptus and trumpet extracts, with a maximum absorbance of approximately 274 nm related to the phytochemical compounds present in the plants that are responsible for the reduction of the precursor ion, such as polyphenols, that are between 250 and 350 nm (Hassane *et al.* 2012). The black solid line shows the iron spectrum obtained, which appears to overlap with the SPR absorption band of zinc NPs at wavelengths from 240 to 390 nm (Devatha *et al.* 2016; Chinnasamy *et al.* 2018; Katata-Seru *et al.* 2018).

3.1.2. Characterization studies of composite FeO/ZnO + SCG

The FTIR spectra shown in Figure 2(a) were conducted to study the functional groups that exist in the samples of eucalyptus–trumpet extract and the presence of organic content on the FeO/ZnO NPs. One of the most prominent peaks is observed around 3,300 cm^{-1} in the three spectra, which is characteristic of the stretching vibration of the O–H groups present in the polyphenols of the extracts. The intensity of this peak decreases considerably after synthesis, suggesting the participation of polyphenols in the reduction of metals (Fe^{2+} and Zn^{2+}) (Liu *et al.* 2018). A weak peak at 2,924 cm^{-1} is attributed to the C–H stretching of the alkanes (Weng *et al.* 2017). The peak value at 2,349 cm^{-1} is due to the C–N stretching vibration (Chauhan *et al.* 2020). The peaks in the region of 1,700–1,000 cm^{-1} are because of the presence of phytochemical

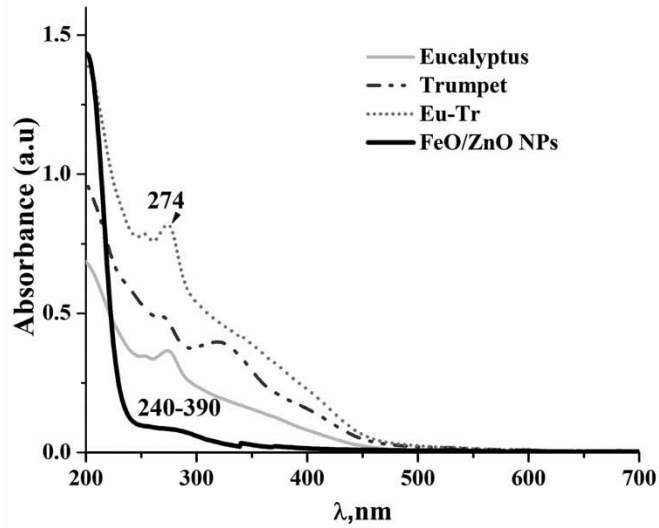

Figure 1 | UV–Vis spectra showing the absorbance of the infusion of Eucalyptus–Trumpet and the solution of the reduction reaction with the metallic salts.

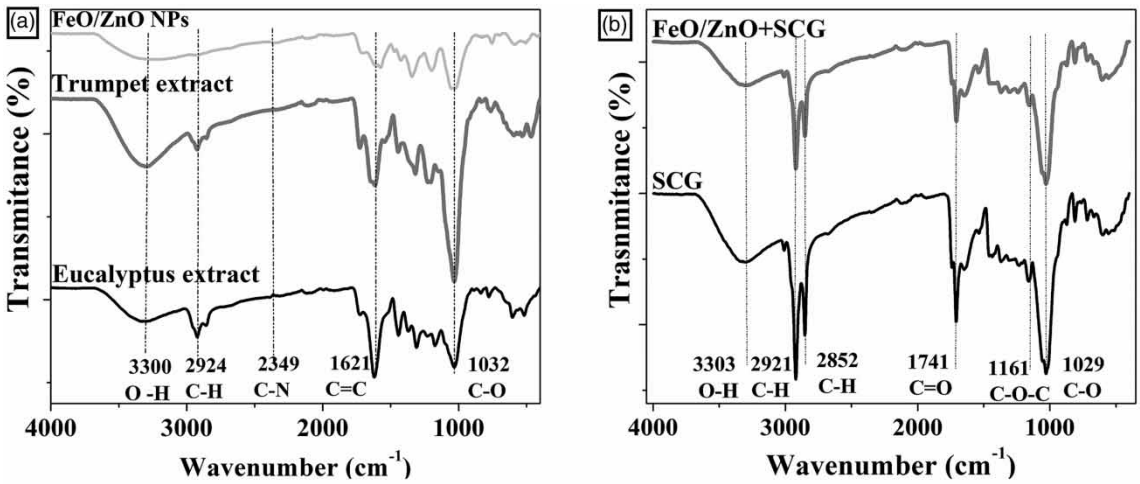

Figure 2 | FTIR spectra for the identification of the functional groups in: (a) Eucalyptus–Trumpet extract and FeO/ZnO nanoparticles and (b) spent coffee grounds (SCGs).

constituents in eucalyptus and trumpet, such as aldehyde, phenol, amine, and alkane compounds (Aik Tan *et al.* 2016; Weng *et al.* 2017; Akbar Jan *et al.* 2021). It is also confirmed that the identified functional groups correspond to eucalyptus extract and trumpet extract.

The presence and shifting peaks in the FeO/ZnO NPs after reduction indicate interaction among the functional groups of the plant extract and the metallic precursors. The reduction and stabilization of NPs are aided by this interaction (Liu *et al.* 2018; Patiño-Ruiz *et al.* 2020). All the peaks below 1,000 cm^{-1} should be attributed to the bonds between inorganic elements and therefore show the presence or absence of NPs (Akbar Jan *et al.* 2021). In this case, one slight peak was observed at 589, indicating the formation of iron oxides due to interaction between the iron and oxygen in the organic compounds (Fe–O) (Devatha *et al.* 2016; Ouyang *et al.* 2019), while the capping layer on the surface of NPs explains the absence of signs of ZnO.

The FTIR shown in Figure 2(b) revealed that SCG is composed of lignocellulosic materials; the sharp band at 1,741 cm^{-1} is associated with carbonyl (C = O) vibration, while an absorption band between 1,700 and 1,500 cm^{-1} may be assigned to the stretching vibration of C–C and C–N (Chien *et al.* 2019).

3.1.3. Scanning electron microscopy (SEM-EDS)

SEM images of FeO/ZnO + SCG in Figure 3(a) revealed the surface morphology of the SCGs, showing highly variable, lumpy, and irregular shapes, which are both attributable to and characteristic of support material. When the NPs are added, a morphological change is not observed, except for the hue change; the bright spots were highly dispersed on the surface, which is attributable to the agglomeration of FeO/ZnO NPs (Chien *et al.* 2019), as shown in Figure 3(b) and 3(c). The EDS spectrum of FeO/ZnO + SCG, shown in Figure 3(d), indicates that it is composed of 7.95% Fe, 8.49 Zn, and 27.95% O, which are part of the NPs, and 55.34% C, 0.45% S, and 0.28% K, which correspond mainly to the support material (SCGs) and possibly to the capping layer of phytochemicals generated during green synthesis (Weng *et al.* 2017).

The TEM analysis shows the presence of different types of NPs in the obtained material. Figure 4(a) shows that the NPs are irregularly shaped and that some are quasi-spherical, which is likely due to differences in the volume ratio of Fe_2O_3 and ZnO, which affected the size and morphology (Noukelag *et al.* 2023). The size distribution was obtained by measuring the size of randomly picked NPs using the ImageJ software; the size distribution histogram is shown in Figure 4(b). The particle sizes ranged from 5 to 30 nm, with an average diameter of 15 nm. It was the polyphenolic compounds present in both extracts that caused the reduction of iron salts to iron NPs. The hydrophobic phenolic compounds attached to the compounds of hydrated Zinc and iron and formed a complex generation of NPs (Obeizi *et al.* 2020; Vitta *et al.* 2020).

The XRD spectrum Figure 5 shows prominent peaks observed at $2\theta = 31.69°$, 34.32°, 36.38°, 47.58°, 46.53°, corresponding to ZnO with planes (1 0 0), (0 0 2), (1 0 1), (1 0 2) and (1 1 0) respectively, which indicate the crystallographic wurtzite structure (JCPDS, card No. 89-7102). The peaks at 24.93°, 33.90°, 39.01°, 40.12° correspond to iron oxide with planes (0 1 2), (1 0 4), (1 1 3) and (0 0 6) respectively, which confirm that the crystalline phase of α-Fe_2O_3-NPs conforms to the standard data JCPDS, JCPDS card No. 01-1030 (Da *et al.* 2018; El-belely *et al.* 2021) and that particles of each compound preserve their crystalline structures. The slight peaks in XRD spectra may be related to the crystallization of organic substances from the green synthesis that coated the surface of NPs (El-belely *et al.* 2021). The data from XRD are compatible with those obtained by TEM, which show an average NP diameter ranging between 20 and 50 nm; these results are similar to previous studies on the biosynthesis of FeO–ZnO NPs (Sathya *et al.* 2018; Masoudinia *et al.* 2021).

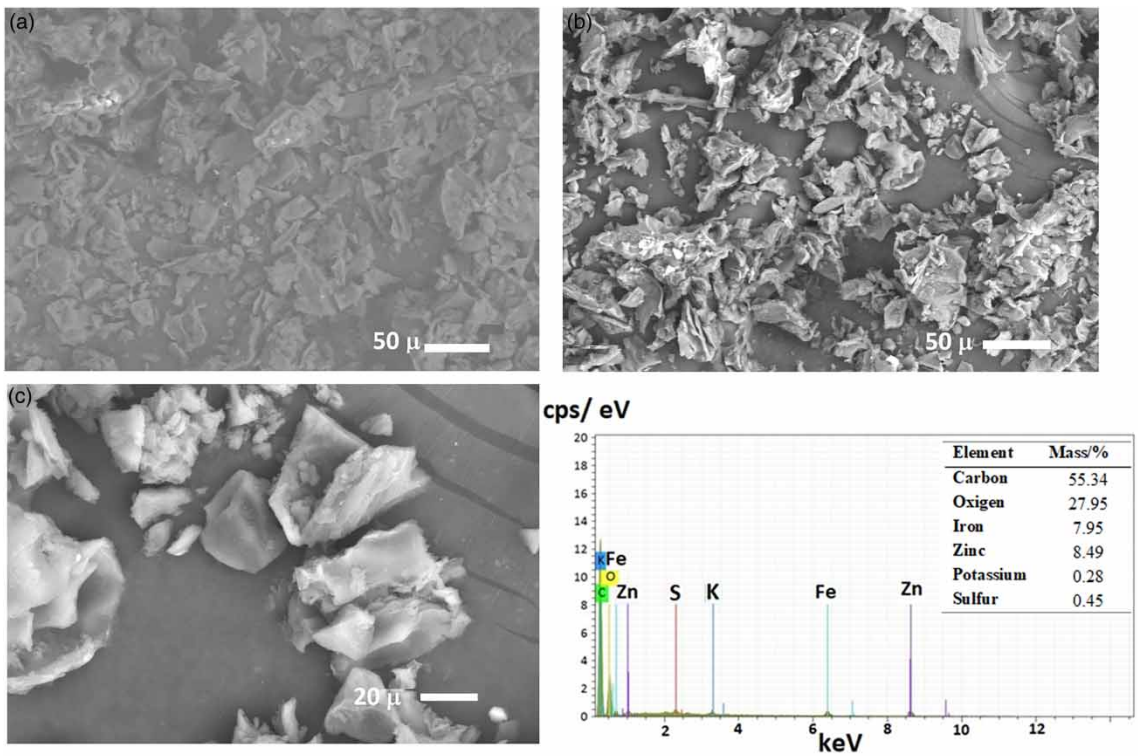

Figure 3 | SEM images of spent coffee grounds (SCGs) (a), FeO/ZnO + SCG (b), FeO/ZnO + SCG different magnifications (c), and EDS analysis (d).

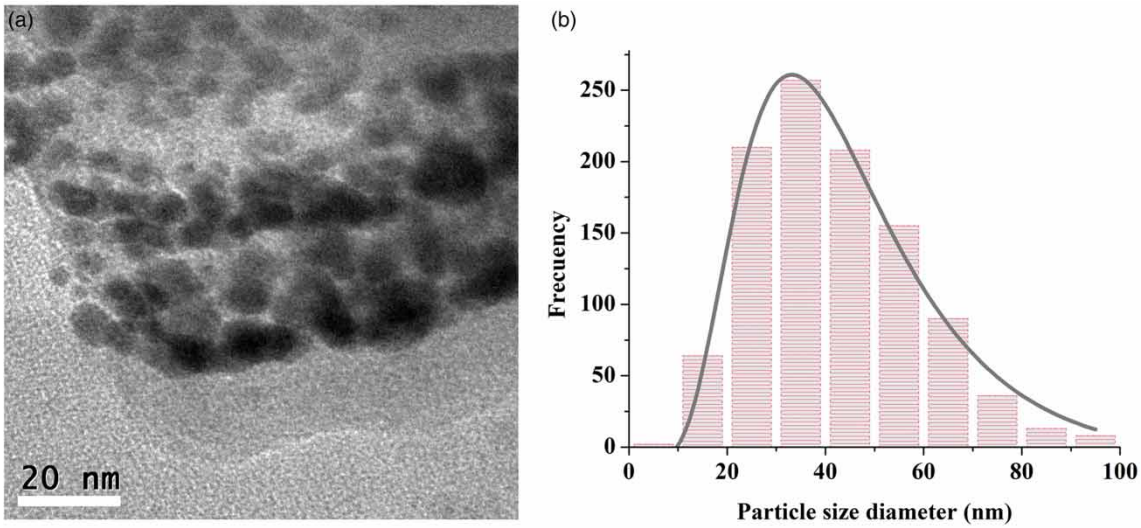

Figure 4 | TEM images of FeO/ZnO nanoparticles (a) and histogram for the particle size distribution (b).

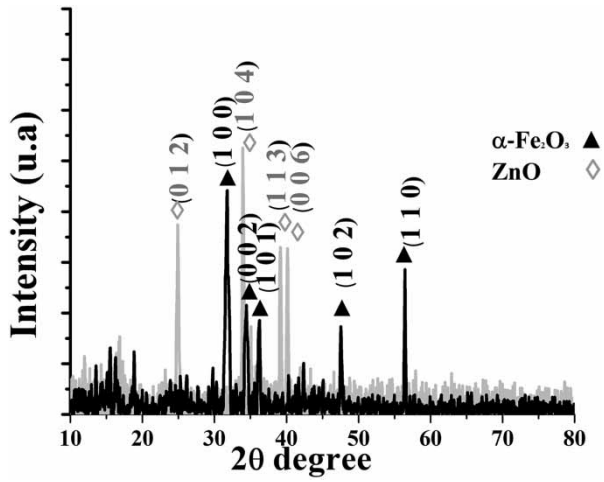

Figure 5 | XRD pattern of FeO/ZnO NPs.

3.2. Fenton-like experiments for the decolorization of indigo carmine dye

3.2.1. Fenton process of indigo carmine dye experiment design

According to the statistical analysis, the experimental data are adjusted to a complete quadratic model with an R^2 of 88.89%. The variance analysis indicates that the factors that have the greatest contribution to the response variable are the quadratic term of the dye concentration ($p < 0.000$), followed by its interaction with the catalyst ($p < 0.000$), and the amount of peroxide added ($p < 0.001$), as shown in the Pareto diagram of standardized effects in Figure 6.

Table 2 shows the ANOVA analysis corresponding to the optimization of the Box–Behnken experimental design. The factors considered were dye concentration (A), catalyst dose (B), and H_2O_2 dose (C). In the Fenton process, the dye concentration was significantly affected at a 5% level of significance. The interactions between dye concentration and catalyst were observed to be significant. The interaction between the catalyst and H_2O_2 was not significant, which suggests the formation of different degradation products when Fe^{3+} was used.

The results of the applied combinations of the Box–Behnken experimental design are presented. The removal efficiency was analyzed for three dye concentrations (50, 75, and 100 mg/L) under different conditions to determine the optimum parameters as shown in Figure 7. The reaction time necessary to remove more than 90% for the lowest concentration was around

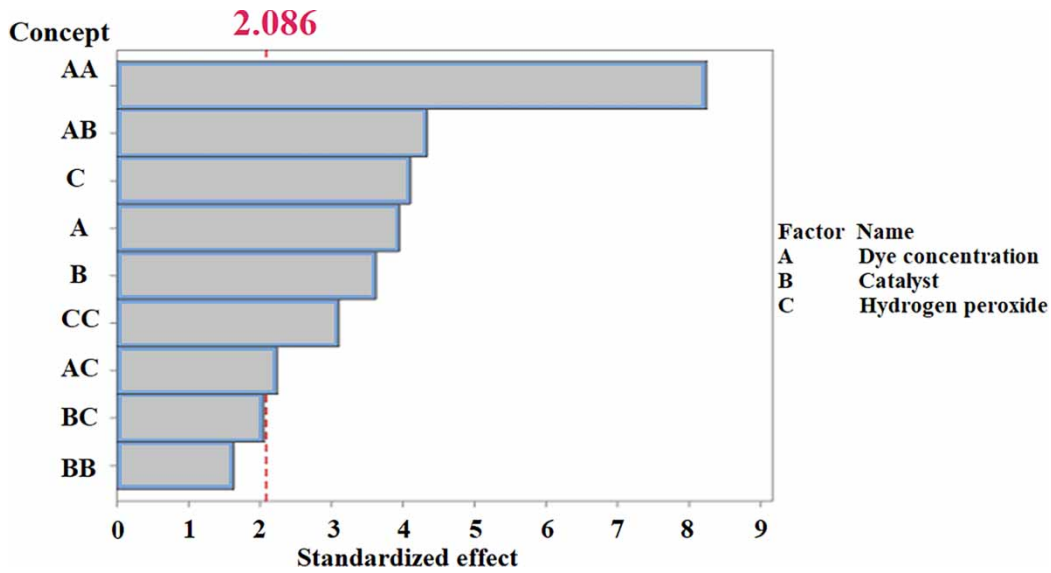

Figure 6 | Pareto diagram of standardized effects (the answer is 120 min, $\alpha = 0.05$).

Table 2 | ANOVA for the optimization of the Box–Behnken experimental design

Source	GL	SC Sec.	Contribution	SC Adj.	MC Adj.	*F*-value	*p*-value
Model	9	77.9175	88.89%	77.918	8.6575	17.79	0.000
Linear	3	22.2782	25.42%	22.278	7.4261	15.26	0.000
(A) Dye concentration	1	7.6300	8.70%	7.630	7.6300	15.68	0.001
(B) Catalyst	1	6.4043	7.31%	6.404	6.4043	13.16	0.002
(C) Hydrogen peroxide	1	8.2438	9.41%	8.244	8.2438	16.94	0.001
Square	3	41.9207	47.83%	41.921	13.9736	28.71	0.000
Dye concentration*Dye concentration	1	36.2618	41.37%	33.086	33.0855	67.97	0.000
Catalyst*Catalyst	1	0.9641	1.10%	1.312	1.3125	2.70	0.116
Hydrogen peroxide*Hydrogen peroxide	1	4.6948	5.36%	4.695	4.6948	9.65	0.006
Two factor interaction	3	13.7186	15.65%	13.719	4.5729	9.39	0.000
Dye concentration*Catalyst	1	9.1916	10.49%	9.192	9.1916	18.88	0.000
Dye concentration*Hydrogen peroxide	1	2.4593	2.81%	2.459	2.4593	5.05	0.036
Catalyst*Hydrogen peroxide	1	2.0677	2.36%	2.068	2.0677	4.25	0.053
Error	20	9.7352	11.11%	9.735	0.4868		
Lack of fit	3	3.3127	3.78%	3.313	1.1042	2.92	0.064
Pure error	17	6.4225	7.33%	6.422	0.3778		
Total	29	87.6527	100.00%				

60 min, while for the highest concentration of indigo carmine (100 mg/L), it was 90 min. When the concentration of the dye is high, dye molecules on the surface of the catalyst are increased, reducing its capacity to generate $OH^{\bullet}$ radicals, and thus the removal efficiency decreases. Also, IC degradation by-products compete with the dye molecule by interacting with $OH^{\bullet}$ radicals, which could be a reason for the decreased removal efficiency (Hassani *et al.* 2018).

The results, in accordance with the design of the experiments, determine that the highest removal efficiencies (95%) for indigo carmine dye occur at pH = 3, H_2O_2 concentration 8.8 mM/L, contact time = 120 min, initial concentration = 69 mg/L, and with 0.5 g/L FeO/ZnO + SCG.

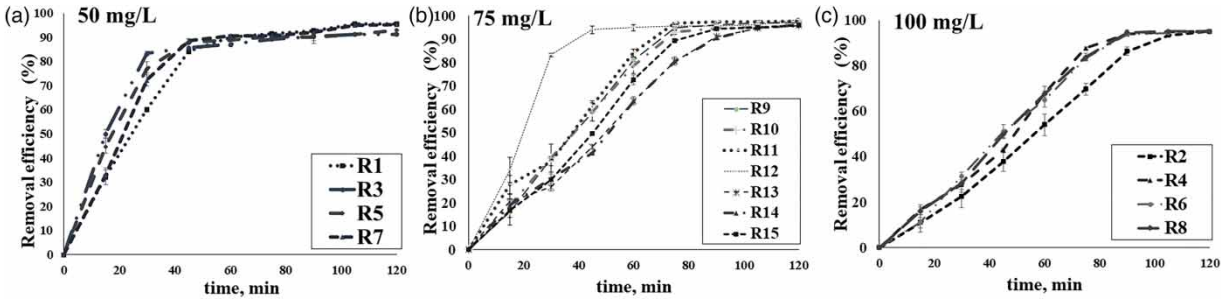

Figure 7 | Effect of dye concentrations of 50, 75, and 100 mg/L. Operating conditions: volume 10 mL, pH 3.0 (Table 1).

Several Fenton investigations have shown that acidic pH levels, close to 3, are normally optimal for Fe oxidations. At low pH levels and in the presence of organic substrates, hydroxyl radicals can abstract a hydrogen atom, initiating the oxidation of Fe. One of the advantages of the Fenton reaction with a solid catalyst is that it reduces sludge generation despite the reaction's reliance on acidic conditions (Gökçe Didar Değermenci 2018; Anil *et al.* 2022; Wakrim *et al.* 2022).

3.2.2. UV–Vis spectrophotometry analysis of experiment design

Figure 8(a) shows the UV–Vis absorbance spectrum of the dye at the beginning and at the end of the treatment, showing the oxidation of the molecule by observing the changes in the maximum absorption waves. In the initial spectrum, a maximum absorbance is observed at λ 610 and at 290 nm, related to the cross-conjugated system or chromophore of C = C and C = O in indigo carmine molecules. This is in addition to λ 252 nm, which corresponds to the absorption of the benzene ring (Lei *et al.* 2021; Abou Seada *et al.* 2022). After the Fenton-like process, the complete elimination of the maximum at 610 nm and the appearance of other signs are observed, specifically a wave at λ 305 nm due to the benzene and carboxylic groups produced by the destruction of the indigoid group and a prominent wave at λ 244 associated with isatin sulfonic acid, which is the main byproduct of IC oxidation (Ray *et al.* 2020). This result indicates that IC is degraded into intermediate compounds.

Batch experiments were conducted to compare the removal efficiencies of indigo carmine through various processes. As shown in Figure 8(b), the FeO/ZnO + SCG composite exhibited relatively low catalytic activity, with only 6.48 ± 1.49% decolorization after 120 min; this suggests that the capacity of the catalyst alone is not significant. The degradation efficiency was approximately 26.60 ± 2.4% for only H_2O_2, due to the access of H_2O_2 molecules to the active sites, resulting in the

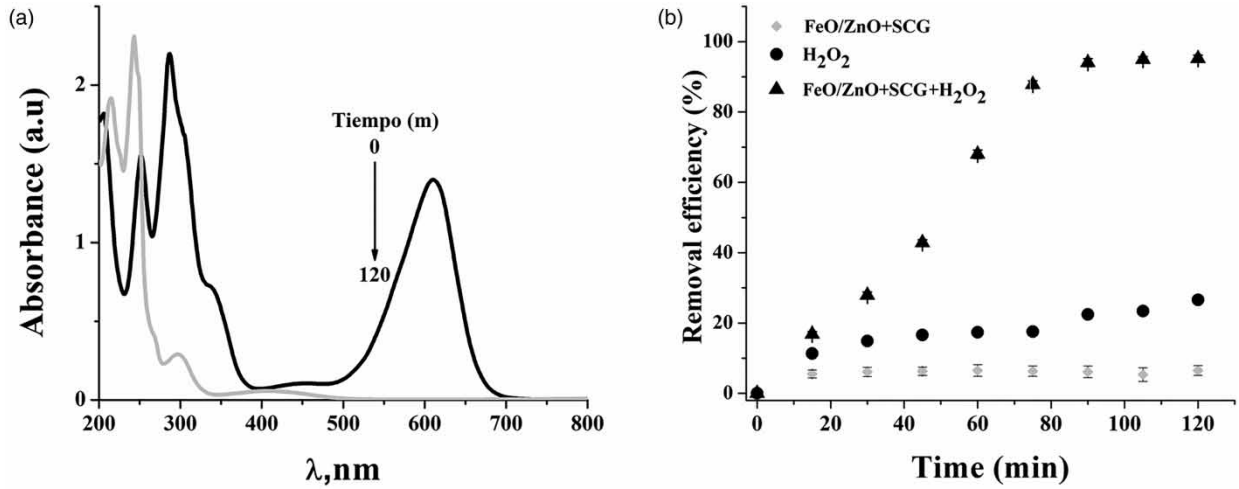

Figure 8 | Study of decolorization with UV–Vis at the beginning and end of the Fenton-like process (a), removal efficiency using H_2O_2 (●), FeO/ZnO + SCG (■), and FeO/ZnO + SCG + H_2O_2 (▲) (b).

generation of OH˙ radicals (Sun *et al.* 2019). The best decolorization yield (95%) was achieved using FeO/ZnO + SCG composites reacting with H_2O_2 for 120 min to form active hydroxyl radicals in the aqueous medium.

Even though the Fenton reaction was initially formulated for Fe(II) and H_2O_2, many redox-active metals such as Zn also display Fenton-like reactions (Dawood & Sen 2014; Fdez-Sanroman *et al.* 2021). The reactions involved in Fenton generate reactive oxygen species derived from the reactions between ferrous ions and hydrogen peroxide (Equations (2) and (3)) (Nagajyothi *et al.* 2020; Thomas *et al.* 2020). The generation of Fe^{2+} on hematite crystal is the key step for the production of active OH˙ radicals (Chan *et al.* 2015).

$$Fe^{2+} + H_2O_2 \rightarrow OH^{\cdot} + OH^{-} + Fe^{3+} \quad (2)$$

$$Fe^{3+} + e^{-} \rightarrow Fe^{2+} \quad (3)$$

Zinc has oxygen-transferring properties for catalytic power and generates highly reactive OH˙ through the Fenton reaction. ZnO NPs have been investigated for applications in the photocatalytic degradation of organic pollutants in wastewater (Yang *et al.* 2022). The Fenton reaction OH˙ is the most powerful oxidant for the oxidative stress in AD. OH˙ is mainly involved in three types of reactions, those being hydrogen abstraction (Equation (4)), addition reaction (Equation (5)) and oxidation reaction equation (Equation (6)) (Das *et al.* 2014).

$$R - H + OH^{\bullet} \rightarrow R + H_2O \quad (4)$$

$$R_4C_2 + OH^{\bullet} \rightarrow R_2 - C(OH) - C - R_2 \quad (5)$$

$$M^{+} + OH^{\bullet} \rightarrow M^{(n1+)} + OH^{-} \quad (6)$$

when ZnO is photo-induced by solar light with photonic energy (*hv)* equal to or greater than the excitation energy (Eg), e^- from the filled valence band (VB) are promoted to an empty conduction band (CB). This process produces electron–hole (e^-/h^+) pairs (Equation (7)), which can migrate to the ZnO surface and be involved in redox reactions as shown in (Equations (8)–(10)), wherein the H^+ reacts with water and hydroxide ions to produce hydroxyl radicals, while the e-reacts with oxygen to produce superoxide radical anions, then hydrogen peroxide (Equations (11) and (12)). Hydrogen peroxide will then react with superoxide radicals to form hydroxyl radicals (Equations (13)–(15)). The hydroxyl radicals are a powerful oxidant that is produced via the Fenton reaction, favoring the attack on pollutants adsorbed on the surface of ZnO to rapidly produce intermediate compounds. Intermediates will eventually be converted into green compounds, such as CO_2, H_2O and mineral acids, as shown in Equations (16) and (17) (Boon *et al.* 2018).

$$Zn \xrightarrow{hv} ZnO(e^{-}_{(CB)}) + (h^{+}_{(VB)}) \quad (7)$$

$$ZnO(h^{+}_{(VB)}) + H_2O \rightarrow ZnO + H^{+} + OH^{\bullet} \quad (8)$$

$$ZnO(h^{+}_{(VB)}) + OH^{-} \rightarrow ZnO + OH^{\bullet} \quad (9)$$

$$ZnO(e^{-}_{(CB)}) + O_2 \rightarrow ZnO + O_2^{\bullet -} \quad (10)$$

$$O_2^{\bullet -} + H^{+} \rightarrow HO_2^{\bullet} \quad (11)$$

$$HO_2^{\bullet} + HO_2^{\bullet} \rightarrow H_2O_2 + O_2 \quad (12)$$

$$ZnO(e^{-}_{(CB)}) + H_2O_2 \rightarrow OH^{\bullet} + OH^{-} \quad (13)$$

$$H_2O_2 + O_2^{\bullet -} \rightarrow OH^{\bullet} + OH^{-} + O_2 \quad (14)$$

$$H_2O_2 + hv \rightarrow 2OH^{\bullet} \quad (15)$$

$$\text{Organic pollutants} + OH^{\bullet} \rightarrow \text{Intermediates} \quad (16)$$

$$\text{Intermediates} \rightarrow CO_2 + H_2O \quad (17)$$

ZnO is a material with high excitation binding energy, but also a wide band gap; it is necessary to irradiate, as the photo-generated electrons from the conduction band (CB) are transferred to the valence band (VB). This results in recombination of the charge carriers to form H_2O molecules, which produces $OH^{\bullet}$ in the valence band that degrades organic compounds. The H_2O_2 was rapidly reduced to $OH^{\bullet}$ for the degradation of the contaminants (Ojha *et al.* 2016).

3.2.3. Zero point charge

The PZC corresponds to the point where the final pH vs. initial pH curve intersects the diagonal. The point zero charge of the FeO/ZnO + SCG composite was 6.35 (Figure 9). Below this pH, the ZnO NPs acquire a positive charge owing to the protonation of functional groups, and above this pH, the surface of the ZnO NPs has a negative charge (Farrokhi *et al.* 2014; Yashni *et al.* 2021). Thus, the composites were positively charged, and adsorption of anionic indigo carmine occurred easily. That is to say, there is electrostatic attraction between the negatively charged indigo carmine functional group and the positively charged amine groups on the surface of the composite.

3.3. Fenton-like process in textile wastewater

Once the best treatment conditions were obtained with the standard solutions for IC, they were applied to a sample from the washing process. The maximum absorbance found was at λ max 671 nm, as shown in Figure 10(a), prior to the initiation of decolorization reactions in the solution. These results indicate that the $OH^{\bullet}$ radical, produced from Fenton reagent, first attacks its C = C double bond, leading to the formation of two molecules of isatin 5-sulfonic acid. Further degradation of isatin 5-sulfonic acid occurs with the release of SO_4^{2-}, and isatin leads to a mixture of oxalic and oxamic acids. The absorption band at 300 nm corresponding to π bonds implies only partial degradation of the molecule (Ammar *et al.* 2006; Ortiz *et al.* 2016; Chowdhury *et al.* 2020).

As illustrated in Figure 10(b), the COD measurement showed that the COD value decreased from 724.5 to 321 mg/L. The remaining COD value in the solution could be due to the presence of intermediates, simpler compounds due to the breakdown of dye, and especially the complex composition of wastewater containing a concentration of recalcitrant organics, metals content and non-soluble substances (Flores *et al.* 2022).

The highest decolorization percentage (approximately 50%) occurs within the first 40 min. As the time increases to 120 min, 88% is achieved, as shown in Figure 9(a).

The Fe–Zn metal ions tend to increase reactive sites, photon adsorption, and the production of hydroxyl radicals. It also had another specific role, as FeO could activate Fenton-like photochemistry, while Zn could delay the electron–hole pair recombination rate, resulting in greater efficiency in the degradation of organic compounds (Talreja *et al.* 2021).

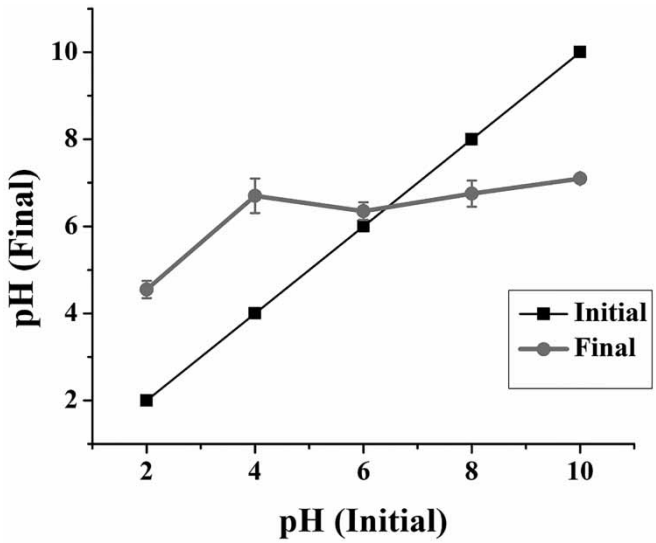

Figure 9 | Point-of-zero charge of FeO/ZnO + SCG.

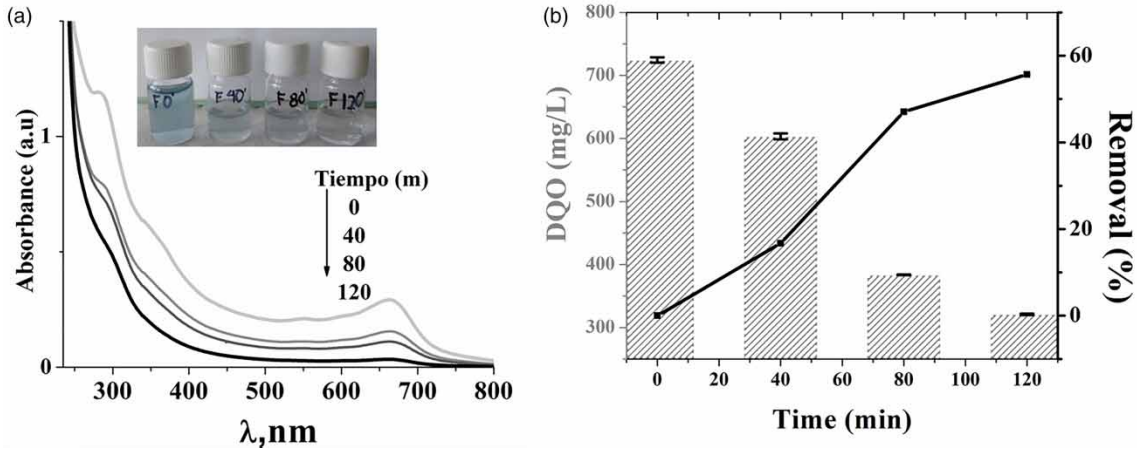

Figure 10 | Variations of UV–vis absorption spectra for IC during the Fenton process (a) and COD removal over time in wastewater treatment (b) ($H_2O_2 = 8.8$ mM/L, FeO/ZnO + SCG = 0.5 g/L, pH = 3.0, $t = 120$ min).

The decolorization and reduction of the chemical oxygen demand decrease when the heterogeneous Fenton-like catalyst is applied, based on the formation of highly reactive hydroxyl radicals ($OH^{\bullet}$) by decomposition of H_2O_2 with Fe^{2+} ions, as shown in Equations (18)–(24).

$$S - Fe^{2+} + H_2O_2 \rightarrow OH^{\bullet} + OH^{-} + S - Fe^{3+} \quad (18)$$

$$S - Fe^{3+} + H_2O_2 \rightarrow S - Fe^{2+} + H^{+} + HO_2^{\bullet} \quad (19)$$

$$S - Fe^{3+} + HO_2^{\bullet} \rightarrow S - Fe^{2+} + H^{+} + O_2 \quad (20)$$

$$S - Fe^{2+} + OH^{\bullet} \rightarrow S - Fe^{3+} + OH^{-} \quad (21)$$

$$OH^{\bullet} + OH^{\bullet} \rightarrow H_2O_2 \quad (22)$$

$$OH^{\bullet} + H_2O_2 \rightarrow H_2O + HO_2^{\bullet} \quad (23)$$

$$OH^{\bullet} + \text{organic molecules} \rightarrow CO_2 + H_2O \quad (24)$$

where S represents the porous solid matrix (SCGs). The ferrous ions initiate the reaction and lead to the generation of hydroxyl radicals. Subsequently, these hydroxyl radicals attack the organic pollutants, causing their degradation (Oruç *et al.* 2019).

Table 3 includes the relevant literature on different composites with metallic NPs that have been applied as catalysts in Fenton-like processes for the removal of dyes. The cases applied in the Fenton process to decolorization dyes show the influence of calcination for obtaining zinc NPs, which is different from the process of this work, reducing time and energy. It has been experimented with mainly in synthetic solutions, in addition to the fact that the dye concentrations are lower than reported in this work.

The efficiency obtained by this work in the Fenton-like experiments is above that reported and compared to the concentrations used by the authors.

4. CONCLUSIONS

The SCGs-supported FeO/ZnO catalyst proposed in this study has been successfully prepared using plant leaf for the first time (*C. aequipetala* Cav). This method is environmentally safer than conventional chemical methods, which is important in terms of process economy for the removal of pollutants from wastewater by heterogeneous Fenton-like processes. XRD, TEM, SEM, FTIR, and EDS validated the synthesis, indicating the obtention of ZnO with a wurtzite structure and a hematite

Table 3 | Comparison with previous works

Preparation method-calcination	Dye concentration	Composite	Decolorization (%)/time	Author
Reduction oxidation method	15 mg/L Textil effluent	Fe^{o}-natural zeolite	94.86%of acid orange 52/180 min	Rashid *et al.* (2020)
Green synthesis	49.6 mg/L Synthetic solution	Fe^{o}-Bentonite-	96.2% of RB 238 dye/180 min	Hassan *et al.* (2020)
Green synthesis	5.0×10^{-5} mol /L Synthetic solution	Fe II-Fe III-SiO_2	100% of Methyl orange/ 180 min	Carvalho & Carvalho (2017)
Heat treatment	49.6 mg/L Synthetic solution	Fe^{o}-polyethylene	Photo–Fenton/100% Ponceau 4R/15 min	Mossmann *et al.* (2019)
Green synthesis (105 °C for 12 h)	100 mg/L Synthetic solution	Fe–Zn-activated carbon	96% of Reactive Red 2/120 min	Oruç *et al.* (2019)
Hydrothermal method	25 mg/L Synthetic solution	Zinc ferrite nanosphere	75.5% of Congo red/3 h	Li *et al.* (2018)
Reduction oxidation method	100 mg/L Synthetic solution	Zn-Fe_2O_4 nanoparticles	94.9% of Orange II/60 min	Cai *et al.* (2016)
Green synthesis (600 °C for 2 h.)	20 mg/L Synthetic solution	$MnFe_2O_4$ nanoparticle	100% of methylene blue/120 min	Chaudhari *et al.* (2022)
Green synthesis	100 mg/L Textil effluent	FeO–ZnO–spend coffe grounds	88% of indigo carmine/ 120min	This work

structure (Fe_2O_3). The combination of FeO/ZnO + SCG and hydrogen peroxide (H_2O_2) in the treatment generated hydroxyl radicals capable of degrading organic matter. The best activity for degradation of indigo carmine was at pH 3, 0.8 g/L of catalyst dosage, and 8.8 mM/L of H_2O_2 for 120 min. This allowed the nanocomposite to be applied in the treatment of residual water from textile dyeing, reducing COD, and color intensity. Thus, nanocomposite is a promising catalyst for the removal of organic dye in the practical application of wastewater treatment.

ACKNOWLEDGEMENTS

The authors gratefully acknowledge Consejo Mexiquense de Ciencia y Tecnología (COMECYT) for the financial support for the research stay EESP2021-0040, and the Centro Conjunto en Química Sustentable UAEMex-UNAM for the infrastructure provided.

DATA AVAILABILITY STATEMENT

All relevant data are included in the paper or its Supplementary Information.

CONFLICT OF INTEREST

The authors declare there is no conflict.

REFERENCES

Abou Seada, N., Ahmed, M. A. & Elmahgary, M. G. 2022 Synthesis and characterization of novel magnetic nanoparticles for photocatalytic degradation of indigo carmine dye. *Materials Science for Energy Technologies* **5**, 116–124.

Aghababai Beni, A. & Jabbari, H. 2022 Nanomaterials for environmental applications. *Results in Engineering* **15**, 100467.

Aik Tan, K., Morad, N. & Ooi, J. Q. 2016 Phytoremediation of methylene blue and methyl orange using eichhornia crassipes. *International Journal of Environmental Science and Development* **7** (10), 724.

Akbar Jan, F., Ullah, R., Ullah, N. & Usman, M. 2021 Exploring the environmental and potential therapeutic applications of Myrtus communis L. assisted synthesized zinc oxide (ZnO) and iron doped zinc oxide (Fe-ZnO) nanoparticles. *Journal of Saudi Chemical Society* **25** (7), 101278.

Albeladi, S. S. R., Malik, M. A. & Al-Thabaiti, S. A. 2020 Facile biofabrication of silver nanoparticles using Salvia officinalis leaf extract and its catalytic activity towards Congo red dye degradation. *Journal of Materials Research and Technology* **9**, 10031–10044.

Ammar, S., Abdelhedi, R., Flox, C., Arias, C. & Brillas, E. 2006 Electrochemical degradation of the dye indigo carmine at boron-doped diamond anode for wastewaters remediation. *Environmental Chemistry Letters* **4**, 229–233.

Anil, G., Scaria, J. & Nidheesh, P. V. 2022 Removal of synthetic dye from aqueous solution using $MnFe_2O_4$-GO catalyzed heterogeneous electro-fenton process. *Water (Switzerland)* **14**, 1–19.

Aragaw, T. A., Bogale, F. M. & Aragaw, B. A. 2021 Iron-based nanoparticles in wastewater treatment: a review on synthesis methods, applications, and removal mechanisms. *Journal of Saudi Chemical Society* **25**, 101280.

Ardila-Leal, L. D., Poutou-Piñales, R. A. & Pedroza-Rodr, A. M. 2021 A brief history of colour, the environmental impact of synthetic dyes and removal by using laccases. *Molecules* **26**, 3813.

Azanaw, A., Birlie, B., Teshome, B. & Jemberie, M. 2022 Textile effluent treatment methods and eco-friendly resolution of textile wastewater. *Case Studies in Chemical and Environmental Engineering* **6**, 100230.

Bel, H., Ali, Z., Bairq, S., Shi, C. & Benzina, M. 2021 Evaluation of sono-assisted solar/Fenton process for indigo carmine degradation over magnetic ZnO-Fe_3O_4 supported Tunisian kaolinite clay. *Surfaces and Interfaces* **26**, 101395.

Benkhaya, S., Rabet, S. M. & El Harfi, A. 2020 A review on classifications, recent synthesis and applications of textile dyes. *Inorganic Chemistry Communications* **115**, 107891.

Boon, C., Yong, L. & Wahab, A. 2018 A review of ZnO nanoparticles as solar photocatalysts : synthesis, mechanisms and applications. *Renewable and Sustainable Energy Reviews* **81**, 536–551.

Cai, C., Zhang, Z., Liu, J., Shan, N., Zhang, H. & Dionysiou, D. D. 2016 Visible light-assisted heterogeneous Fenton with $ZnFe_2O_4$ for the degradation of Orange II in water. *Applied Catalysis B: Environmental* **182**, 456–468.

Carvalho, S. S. F. & Carvalho, N. M. F. 2017 Dye degradation by green heterogeneous Fenton catalysts prepared in presence of Camellia sinensis. *Journal of Environmental Management* **187**, 82–88.

Cesur Özcan, E. N. & Gürel, L. 2023 A comparison for the removal of two different textile dyes by raw Helianthus annuus L. seed shells. *International Journal of Environmental Science and Technology* **20** (6), 6791–6804.

Chan, J. Y. T., Ang, S. Y., Ye, E. Y., Sullivan, M., Zhang, J. Y. & Lin, M. 2015 Heterogeneous photo-Fenton reaction on hematite (α-Fe_2O_3){104},{113} and {001} surface facets. *Physical Chemistry Chemical Physics* **17** (38), 25333–25341.

Chaudhari, A., Kaida, T., Desai, H. B., Ghosh, S., Bhatt, R. P. & Tanna, A. R. 2022 Dye degradation and antimicrobial applications of manganese ferrite nanoparticles synthesized by plant extracts. *Chemical Physics Impact* **5**, 100098.

Chauhan, A. K., Kataria, N. & Garg, V. K. 2020 Green fabrication of ZnO nanoparticles using Eucalyptus spp. leaves extract and their application in wastewater remediation. *Chemosphere* **247**, 125803.

Chien, H.-W., Kuo, C.-J., Kao, L.-H., Lin, G.-Y. & Chen, P.-Y. 2019 Polysaccharidic spent coffee grounds for silver nanoparticle immobilization as a green and highly efficient biocide. *International Journal of Biological Macromolecules* **140**, 168–176.

Chinnasamy, C., Tamilselvam, P., Karthick, B., Sidharth, B. & Senthilnathan, M. 2018 Green synthesis, characterization and optimization studies of zinc oxide nano particles using costusigneus leaf extract. *Materials Today: Proceedings* **5**, 6728–6735.

Chowdhury, M., Khandaker, S., Sarker, F. & Islam, A. 2020 Current treatment technologies and mechanisms for removal of indigo carmine dyes from wastewater : a review. *Journal of Molecular Liquids* **318**, 114061.

Da, E., Taha, A. & Afkar, E. 2018 Applied sciences green synthesis of iron nanoparticles by Acacia nilotica pods extract and Its catalytic, adsorption, and antibacterial activities. *Applied Sciences (Switzerland)* **8**, 1922.

Das, T. K., Wati, M. R. & Fatima-shad, K. 2014 Oxidative stress gated by fenton and haber weiss reactions and its association with Alzheimer ' s disease. *Arch Neurosci* **2**, e20078.

Dawood, S. & Sen, T. K. 2014 Review on dye removal from its aqueous solution into alternative cost effective and non-conventional adsorbents. *J Chem Proc Eng* **1**, 104.

Devatha, C. P., Thalla, A. K. & Katte, S. Y. 2016 Green synthesis of iron nanoparticles using different leaf extracts for treatment of domestic waste water. *Journal of Cleaner Production* **139**, 1425–1435.

Długosz, O., Szostak, K., Krupiński, M. & Banach, M. 2021 Synthesis of Fe_3O_4/ZnO nanoparticles and their application for the photodegradation of anionic and cationic dyes. *International Journal of Environmental Science and Technology* **18**, 561–574.

El-belely, E. F., Farag, M. M., Said, H. A., Amin, A. S., Azab, E., Gobouri, A. A. & Fouda, A. 2021 Green synthesis of zinc oxide nanoparticles (ZnO-NPs) using arthrospira platensis (Class : Cyanophyceae) and evaluation of their biomedical activities. *Nanomaterials* **11**, 95.

Elsehly, E., Alruqic, A. B., Khouly, A. E.-, Khoavaylo, V. & Alqannas, H. 2023 Thermoelectric performance of Fe_2 ALV/CNT-based alloys. *Thermal Science* **27**, 389–396.

Farrokhi, M., Hosseini, S. C., Yang, J. K. & Shirzad-Siboni, M. 2014 Application of ZnO-Fe_3O_4 nanocomposite on the removal of azo dye from aqueous solutions: kinetics and equilibrium studies. *Water, Air, and Soil Pollution* **225**, 1–12.

Fdez-Sanroman, A., Martinez-Treinta, R., Rosalez, E. & Sanroman, M. 2021 Applied sciences heterogeneous electro-Fenton-like designs for the disposal of 2-Phenylphenol from water. *Applied Sciences* **11**, 12103.

Ferrier, D. C., Kiely, J. & Luxton, R. 2022 Metal oxide decorated carbon nanocomposite electrodes for propofol monitoring. *Biosensors and Bioelectronics* **X 12**, 100286.

Flores, M. A. D., Revilla Pacheco, C., Garcia Bustos, K., Tejada Meza, K., Terán-Hilares, F., Pacheco Tanaka, D. A. & Terán-Hilares, R. 2022 Efficient dye removal from real textile wastewater using orange seed powder as suitable bio-adsorbent and membrane technology. *Water* **14**, 4104.

Gökçe Didar Değermenci 2018 Decolorization of reactive azo dye by fenton and photo-fenton processes in aqueous solution: the influence of operating conditions, kinetics study, and performance comparison. *Bulletin of the Chemical Society of Ethiopia* **3**, 10–27.

Hassan, A. K., Al-Kindi, G. Y. & Ghanim, D. 2020 Green synthesis of bentonite-supported iron nanoparticles as a heterogeneous Fenton-like catalyst: kinetics of decolorization of reactive blue 238 dye. *Water Science and Engineering* **13**, 286–298.

Hassane, E., Gierschner, J., Duroux, J.-l. & Trouillas, P. 2012 UV/visible spectra of natural polyphenols : a time-dependent density functional theory study. *Food Chemistry* **131**, 79–89.

Hassani, A., Çelikdağ, G., Eghbali, P., Sevim, M., Karaca, S. & Metin, Ö. 2018 Heterogeneous sono-Fenton-like process using magnetic cobalt ferrite-reduced graphene oxide ($CoFe_2O_4$-rGO) nanocomposite for the removal of organic dyes from aqueous solution. *Ultrasonics – Sonochemistry* **40**, 841–852.

Hevira, L., Ighalo, J. O. & Zein, R. 2020 Biosorption of indigo carmine from aqueous solution by *Terminalia Catappa* shell. *Journal of Environmental Chemical Engineering* **8**, 104290.

Jiménez-Rosado, M., Gomez-Zavaglia, A., Guerrero, A. & Romero, A. 2022 Green synthesis of ZnO nanoparticles using polyphenol extracts from pepper waste (Capsicum annuum). *Journal of Cleaner Production* **350**, 131541.

Jin, L., Zhang, H. & Ma, Z. 2018 Study on capacity of coffee grounds to be extracted oil, produce biodiesel and combust. *Energy Procedia* **152**, 1296–1301.

Katata-Seru, L., Moremedi, T., Aremu, O. S. & Bahadur, I. 2018 Green synthesis of iron nanoparticles using Moringa oleifera extracts and their applications: removal of nitrate from water and antibacterial activity against Escherichia coli. *Journal of Molecular Liquids* **256**, 296–304.

Kumar, V., Kaushal, A., Shah, M. P. & Singh, K. 2021 *Chapter 16 - Phytoaugmentation Technology for Phytoremediation of Environmental Pollutants: Current Scenario and Future Prospects*. Elsevier B.V., Uttar Pradesh, India, pp. 329–381.

Lei, J., Zhang, Y. & He, P. 2021 An α-fe2o3/circulating fluidized bed fly ash based geopolymer composite anode for electrocatalytic degradation of indigo carmine dye wastewater. *Journal of Renewable Materials* **9**, 2277–2289.

Li, Y., Chen, D., Fan, S. & Yang, T. 2018 Metal-doped zinc ferrite nanosphere prepared from metal-rich industrial wastewater. *Journal of the Taiwan Institute of Chemical Engineers* **96**, 185–192.

Liang, C., Cheong, J. Y., Sitaru, G., Rosenfeldt, S., Schenk, A. S., Gekle, S. & Greiner, A. 2022 Size-dependent catalytic behavior of gold nanoparticles. *Advanced Materials Interfaces* **9** (4), 2100867.

Liu, Y., Jin, X. & Chen, Z. 2018 The formation of iron nanoparticles by Eucalyptus leaf extract and used to remove Cr(VI). *Science of the Total Environment* **627**, 470–479.

Mangindaan, D., Lin, G.-Y., Kuo, C.-J. & Chien, H.-W. 2020 Biosynthesis of silver nanoparticles as catalyst by spent coffee ground/recycled poly(ethylene terephthalate) composites. *Food and Bioproducts Processing* **121**, 193–201.

Martınez-Bonfil, B., Hernandez, A. C., Laredo, A. L., Tapia, G. T. & Espino, J. T. 2014 Effects of culture medium and auxins on growth of adventitious root cultures of Cuphea aequipetala Cav . and their ability to produce antioxidant compounds. *Plant Cell, Tissue and Organ Culture (PCTOC)* **118**, 401–408.

Masoudinia, M., Badoei-dalfard, A., Ravan, H. & Karami, Z. 2021 CHEMISTRY fabrication and characterization of the green synthesized magnetic chitosan-zinc nanocomposites : a reusable and effective multifunctional nanocatalyst for the. *Analytical and Bioanalytical Chemestry Research* **8**, 385–403.

Mossmann, A., Dotto, G. L., Hotza, D., Jahn, S. L. & Foletto, E. L. 2019 Preparation of polyethylene-supported zero-valent iron buoyant catalyst and its performance for Ponceau 4R decolorization by photo-Fenton process. *Journal of Environmental Chemical Engineering* **7**, 102963.

Mousset, E., Trellu, C. & Oturan, M. A. 2021 Electrochemical technologies coupled with biological treatments. *Current Opinion in Electrochemistry, Elsevier* **26**, 100668.

Nadeem, N., Zahid, M., Tabasum, A., Mansha, A., Jilani, A., Bhatti, I. A. & Bhatti, H. N. 2020 Degradation of reactive dye using heterogeneous photo-Fenton catalysts : $ZnFe_2O_4$ and GO-. *Materials Research Express PAPER* **7**, 015519.

Nagajyothi, P. C., Prabhakar Vattikuti, S. V., Devarayapalli, K. C., Yoo, K., Shim, J. & Sreekanth, T. V. M. 2020 Green synthesis: photocatalytic degradation of textile dyes using metal and metal oxide nanoparticles-latest trends and advancements. *Critical Reviews in Environmental Science and Technology* **50**, 2617–2723.

Nagar, N. & Devra, V. 2018 Green synthesis and characterization of copper nanoparticles using Azadirachta indica leaves. *Materials Chemistry and Physics* **213**, 44–51.

Nair, G. M., Sajini, T. & Mathew, B. 2022 Advanced green approaches for metal and metal oxide nanoparticles synthesis and their environmental applications. *Talanta Open* **5**, 100080.

Nasrollahzadeh, M., Sajjadi, M., Dadashi, J. & Ghafuri, H. 2020 Mechanism, stability, catalytic and antimicrobial activities. *Advances in Colloid and Interface Science* **276**, 102103.

Noukelag, S. K., Cummings, F. & Arendse, C. J. 2023 Physical and magnetic properties of biosynthesized ZnO/Fe_2O_3, $ZnO/ZnFe_2O_4$, and $ZnFe_2O_4$ nanoparticles. *Results in Surfaces and Interfaces* **10**, 100092.

Obeizi, Z., Benbouzid, H., Ouchenane, S., Yılmaz, D., Culha, M. & Bououdina, M. 2020 Biosynthesis of Zinc oxide nanoparticles from essential oil of Eucalyptus globulus with antimicrobial and anti-bio fi lm activities. *Materials Today Communications Journal* **25**, 101553.

Ojha, D. P., Joshi, M. K. & Joo, H. 2016 Photo-Fenton degradation of organic pollutants using a zinc oxide decorated iron oxide/reduced graphene oxide nanocomposite. *Ceramics International* **43** (1), 1290–1297.

Oliveira, M. T., Garcia, L. F., Siqueira, A. C. R., Somerset, V. & Gil, E. S. 2020 Electrocoagulation of the indigo carmine dye using electrodes produced from the compression of metallurgical filing wastes. *International Journal of Environmental Science and Technology* **17**, 1657–1662.

Ortiz, E., Gómez-Chávez, V., Cortés-Romero, C. M., Solís, H. & Ruiz-Ramos, R. 2016 Degradation of indigo carmine using advanced oxidation processes : synergy effects and toxicological study. *Scientific Research Publishing*. https://doi.org/10.4236/jep.2016.712137.

Oruç, Z., Ergüt, M., Uzuno, D. & Özer, A. 2019 Green synthesis of biomass-derived activated carbon/Fe-Zn bimetallic nanoparticles from lemon wastes for heterogeneous Fenton-like decolorization of Reactive Red 2. 7. *Journal of Environmental Chemical Engineering* **7** (4), 103231.

Ouyang, Q., Kou, F., Tsang, P. E., Lian, J., Xian, J., Fang, J. & Fang, Z. 2019 Green synthesis of Fe-based material using tea polyphenols and its application as a heterogeneous Fenton-like catalyst for the degradation of lincomycin. *Journal of Cleaner Production* **232**, 1492–1498.

Patiño-Ruiz, D., Sanchez-Botero, L., Tejeda-Benitez, L. & Hinestroza, J. 2020 Green synthesis of iron oxide nanoparticles using Cymbopogon citratus extract and sodium carbonate salt: Nanotoxicological considerations for potential environmental applications David Patiño-Ruiz. *Environmental Nanotechnology, Monitoring & Management* **14**, 1–39.

Peramune, D., Manatunga, D. C., Dassanayake, R. S., Premalal, V., Liyanage, R. N., Gunathilake, C. & Abidi, N. 2022 Recent advances in biopolymer-based advanced oxidation processes for dye removal applications: a review. *Environmental Research* **215**, 114242.

Rashid, T., Iqbal, D., Hazafa, A., Hussain, S., Sher, F. & Sher, F. 2020 Formulation of zeolite supported nano-metallic catalyst and applications in textile effluent treatment. *Journal of Environmental Chemical Engineering* **8**, 104023.

Ray, S. K., Dhakal, D. & Lee, S. W. 2020 Visible light driven Ni–BaMo3O10 photocatalyst for Indigo Carmine degradation: mechanism and pathways. *Materials Science in Semiconductor Processing* **105**, 104697.

Sathya, K., Saravanathamizhan, R. & Baskar, G. 2018 Ultrasonic assisted green synthesis of Fe and Fe/Zn bimetallic nanoparticles for invitro cytotoxicity study against HeLa cancer cell line. *Molecular Biology Reports* **45** (5), 1397–1404.

Scaria, J., Nidheesh, P. V. & Kumar, M. S. 2020 Synthesis and applications of various bimetallic nanomaterials in water and wastewater treatment. *Journal of Environmental Management* **259**, 110011.

Siripireddy, B. & Mandal, B. K. 2017 Facile green synthesis of zinc oxide nanoparticles by Eucalyptus globulus and their photocatalytic and antioxidant activity. *Advanced Powder Technology* **28**, 785–797.

Sun, Y., Yang, Z., Tian, P., Sheng, Y., Xu, J. Y. & Han, Y. F. 2019 Oxidative degradation of nitrobenzene by a Fenton-like reaction with Fe-Cu bimetallic catalysts. *Applied Catalysis B: Environmental* **244**, 1–10.

Sun, Y., Zhang, W., Li, Q., Liu, H. & Wang, X. 2023 Preparations and applications of zinc oxide based photocatalytic materials. *Advanced Sensor and Energy Materials* **2**, 100069.

Talreja, N., Afreen, S., Ashfaq, M. & Chauhan, D. 2021 Chemosphere bimetal (Fe/Zn) doped BiOI photocatalyst : an effective photodegradation of tetracycline and bacteria. *Chemosphere* **280**, 130803.

Thomas, N., Dionysiou, D. & Pillai, S. 2020 Heterogeneous Fenton catalysts: a review of recent advances. *Journal of Hazardous Materials* **404**, 124082.

Vitta, Y., Figueroa, M., Calderon, M. & Ciangherotti, C. 2020 Synthesis of iron nanoparticles from aqueous extract of eucalyptus robusta Sm and evaluation of antioxidant and antimicrobial activity. *Materials for Energy Technologies* **3**, 97–103.

Wakrim, A., Zaroual, Z., El Ghachtouli, S., Jamal Eddine, J. & Azzi, M. 2022 Treatment and degradation of azo dye waste industry by electro-fenton process. *Physical Chemistry Research* **10**, 495–504.

Weng, X., Guo, M., Luo, F. & Chen, Z. 2017 One-step green synthesis of bimetallic Fe/Ni nanoparticles by eucalyptus leaf extract: biomolecules identification, characterization and catalytic activity. *Chemical Engineering Journal* **308**, 904–911.

Wu, C.-T., Agrawal, D. C., Huang, W. Y., Hsu, H. C., Yang, S. J., Huang, S. L. & Lin, Y. S. 2019 Functionality analysis of spent coffee ground extracts obtained by the hydrothermal method. *Journal of Chemistry* **2019**, 1–8.

Xiao, C., Li, H., Zhao, Y., Zhang, X. & Wang, X. 2020 Green synthesis of iron nanoparticle by tea extract (polyphenols) and its selective removal of cationic dyes. *Journal of Environmental Management* **275**, 111262.

Yang, Y.-c., Sahu, R. S. & Shih, Y.-h. 2022 Influence of aqueous chloride and bromide ions on bisphenol A degradation efficiency with zinc oxide nanoparticles. *Sustainable Environment Research* **1**, 32. 12.

Yaseen, D. A. & Scholz, M. 2019 Textile Dye Wastewater Characteristics and Constituents of Synthetic Effluents: A Critical Review. *International Journal of Environmental Science and Technology* **16**, 1193–1226.

Yashni, G., Al-Gheethi, A., Mohamed, R. & Al-Sahari, M. 2021 Reusability performance of green zinc oxide nanoparticles for photocatalysis of bathroom greywater. *Water Practice and Technology* **16**, 364–376.

First received 12 May 2023; accepted in revised form 23 August 2023. Available online 6 September 2023